J. Fluid Mech. (2013), *vol.* 717, *pp.* 255–280.
doi:10.1017/jfm.2012.569

Three-vortex quasi-geostrophic dynamics in a two-layer fluid. Part 2. Regular and chaotic advection around the perturbed steady states

K. V. Koshel[1,2],†, **M. A. Sokolovskiy**[3,4] **and J. Verron**[5]

[1]V.I. Il'ichev Pacific Oceanological Institute, FEB RAS, 43 Baltiyskaya Str., Vladivostok, 690041, Russia
[2]Far Eastern Federal University, 8 Sukhanova Str., Vladivostok, 690950, Russia
[3]Water Problems Institute, RAS, 3 Gubkina Str., Moscow, 119333, Russia
[4]Southern Federal University, 8a Mil'chakova Str., Rostov-on-Don, 344090, Russia
[5]Laboratoire des Ecoulements Géophysiques et Industriels, CNRS, BP 52, 38041, Grenoble, CEDEX 9, France

(Received 18 March 2012; revised 11 November 2012; accepted 15 November 2012; first published online 1 February 2013)

We study fluid-particle motion in the velocity field induced by a quasi-stationary point vortex structure consisting of one upper-layer vortex and two identical vortices in the bottom layer of a rotating two-layer fluid. The regular regimes are investigated, and the possibility of chaotic regimes (chaotic advection) under the effect of quite small non-stationary disturbances of stationary configurations has been shown. Examples of different scenarios are given for the origin and development of chaos. We analyse the role played by the stochastic layer in the processes of mixing and in the capture of fluid particles within a vortex area. We also study the influence of stratification on these effects. It is shown that regular and chaotic advection situations exhibit significant differences in the two layers.

Key words: baroclinic flows, mixing and dispersion, quasi-geostrophic flows

1. Introduction

The motion of fluid particles (advection) in a vortex field is of serious interest both for studying mixing processes and for investigating different aspects of turbulence. The problem of advection of fluid particles in the velocity field induced by barotropic vortex structures has attracted the attention of researchers for more than 30 years. The papers by Aref & Pomphrey (1980), Aref (1983), Neu (1984), Aref (1986), Eckhardt & Aref (1988), Aref *et al.* (1989), Polvani & Wisdom (1990), Oliva (1991), Polvani & Plumb (1992), Meleshko *et al.* (1992), Meleshko & Konstantinov (1993), Velasco Fuentes (1994), Velasco Fuentes, van Heijst & Cremers (1995), Péntek, Tél & Toroczkai (1995), Kuznetsov & Zaslavsky (1998, 2000), Boatto & Pierrehumbert (1999), Leoncini, Kuznetsov & Zaslavsky (2000, 2001), Leoncini & Zaslavsky (2002) and Koshel & Prants (2006) provide a representative sample.

† Email address for correspondence: kvkoshel@poi.dvo.ru

In natural geophysical media and in particular in the ocean, vertical stratification plays a very important role and obviously affects advective processes. Here, as a first step in the investigation of this effect, we consider the specific features of fluid-particle motion around the perturbed steady states of vortex structures in a two-layer rotating fluid obtained by Gryanik (1988), Sokolovskiy & Verron (2000, 2002*a*,*b*, 2004, 2006), Gryanik, Sokolovskiy & Verron (2006), Kizner (2006) and Jamaloodeen & Newton (2007).

In the present work, we show that the two-layer quasi-stationary vortex structures obtained in an accompanying paper (Sokolovskiy, Koshel & Verron 2013, hereinafter referred to as SKV) can trap and transport considerable volumes of fluid in both layers. Following Thomson (1867), we will refer to the volume of the trapped fluid as the *vortex atmosphere*. In addition to estimating the volume of fluid captured and transported by vortex structures, which is of interest *per se* in the context of analysis of oceanic or atmospheric processes, this study will serve as a basis for establishing the conditions under which chaotic motion of fluid particles can appear, resulting in mixing and mass exchange between the vortex atmosphere and adjacent domains.

There are numerous works where some methods of analysis of the two-dimensional chaotic movements have been used for explaining natural phenomena. We will next cite some of them of particular relevance.

The problem of kinematic barriers, which are identified with KAM-tori of the respective dynamic systems, has been discussed by Cox *et al.* (1990), Yang (1993, 1996*b*, 1998), Ngan & Shepherd (1997), Koshel & Prants (2006) and Budyansky *et al.* (2009) in the context of the interaction between a jet stream and a Rossby wave, and in studies by Yang & Liu (1994, 1997), Yang (1996*a*) and Perrot & Carton (2009) applied to the contact zone between two large oceanic vortices.

Abraham & Bowen (2002), using the maximum cross-correlation method, performed an analysis of the surface velocity field in a region of the East Australian Current (between latitudes 36 °S and 41 °S and longitudes 150 °E and 156 °E) which allowed them to explain the peculiarities of satellite imagery of sea-surface temperature and chlorophyll distributions in this ocean area.

Neufeld *et al.* (2002) note that stirring imposes a filamentary structure of phytoplankton bloom arising due to the irregular chaotic motion of fluid elements, known as *chaotic advection* introduced by Aref (1984).

Our analysis of the likelihood of chaotic regime formation is based on the methods explained in particular by Izrailsky, Koshel & Stepanov (2006, 2008) and Koshel, Sokolovskiy & Davies (2008) (applied in this paper to a two-layer rotating fluid) and requires studying the spatial distributions of the turnover frequency of fluid particles in the vortex atmosphere.

We believe that the model proposed in this work may be useful for understanding mixing in the Earth's stratified oceans, atmosphere and magma, and for explaining meandering of jet currents and deep convection. Analysis methods of advective processes, proposed in this article, may be particularly useful when studying regular and chaotic motion of ARGOS drift buoys (Rogachev & Carmack 2002) or thermohaline transitions in the vicinity of quasi-vortex structures in the ocean (Rogachev 2000).

The structure of the paper is as follows. In § 2, we discuss the regular advection in the vicinity of a stationary two-layer configuration of a three-point-vortex *roundabout*, find the role of geometric parameters (§ 2.1) and of the intensity μ of the upper-layer vortex (§ 2.2); in § 2.3, a particular case of a *triton* ($\mu = -2$) is studied in detail.

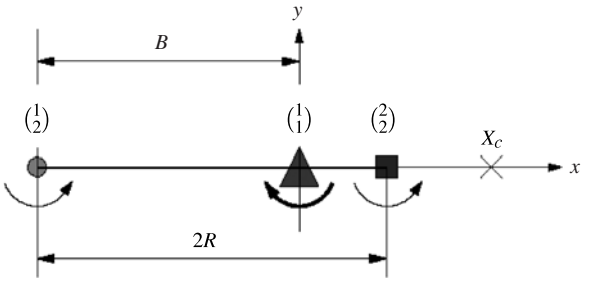

FIGURE 1. Scheme of the initial collinear layout of vortices for the case $B > R$. The triangle marks the position of the top-layer vortex and the circle and square mark the positions of the bottom-layer vortices; X_c is the position of the centre of rotation given by (3.4) in SKV. The size of each symbol is proportional to the absolute value of the intensity of the vortex. The arc arrows show the cyclonic or anticyclonic directions of vortices.

Section 3 is devoted to the investigation of the characteristics of chaotic advection in the vicinity of a perturbed triton. In § 4, we present our main results.

2. Regular advection in the vicinity of stationary configurations

We focus now on the advection of fluid particles in a velocity field induced by the stationary vortex structures in the framework of the inviscid, quasi-geostrophic, two-layer, f-plane model described in the accompanying paper SKV. These co-propagating or co-rotating stationary structures consist of two identical point vortices in the bottom layer and one point vortex in the top layer. Here, as in SKV, we will use the notation $\binom{\alpha}{i}$ for the point vortex with dimensionless circulation κ_i^α and coordinates (x_i^α, y_i^α) where the lower index corresponds to number of the layer ($i = 1, 2$) and the upper index corresponds to number of the vortex ($\alpha = 1, 2, \ldots, A_i$). As in SKV, we suppose now $A_1 = 1, A_2 = 2$, $\kappa_1^1 = \mu$, $\kappa_2^1 = \kappa_2^2 = 1$.

Let us also consider that the initial layout of the vortices is the collinear one as shown in figure 1.

In a steady case, the trajectories of motion of material particles coincide with the streamlines of horizontal motion, and the simplest method of studying the motion of particles is to introduce point vortices with zero intensity. By analogy with the above reasoning, we will pay special attention to studying the behaviour of the turnover frequency Ω of fluid particles in the vortex flow ($\Omega = 2\pi/T$, where T is the rotation period of a particle about an elliptic point of a phase space), an important characteristic of the chaotic properties of advection processes (Izrailsky *et al.* 2006, 2008; Koshel *et al.* 2008). Numerical experiments for studying the motion of fluid particles were carried out using the standard Bulirsch–Stoer method of fourth-order accuracy.

2.1. *Dependence on B and R on* $\mu = -2.5$

We will start our analysis from the case $B = R = R_0^{(r)}$ (see the notation in figure 1), i.e. a symmetrical roundabout. Recall that $R_0^{(r)}$ denotes the distance between the central vortex of the upper layer and the peripheral vortices of the bottom layer when $\omega = 0$ is the solution of equation (3.1) in SKV.

Figure 2 shows phase portraits for the top and bottom layers with $\mu = -2.5$. The lateral cyclonic formations in the top layer are obviously induced by peripheral

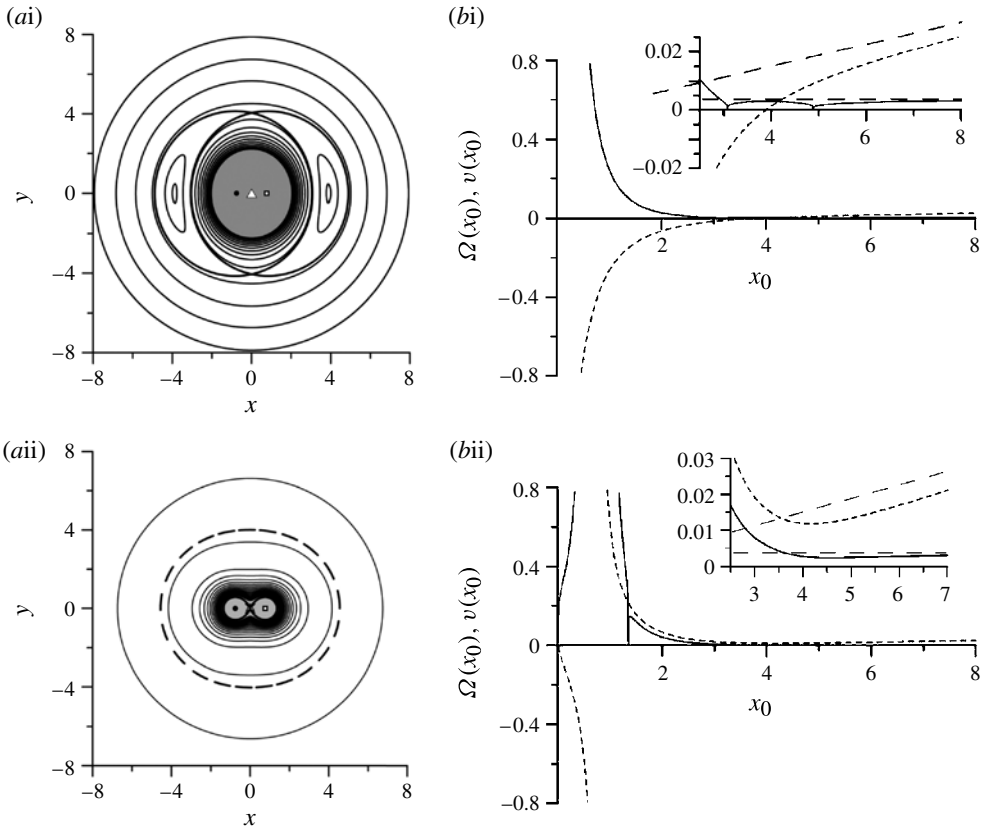

FIGURE 2. (*a*) Isolines of the stream-function in a co-rotated coordinate system with $\mu = -2.5$ and $B = R = R_0^{(r)} = 0.7609$ in the top (i) and bottom (ii) layers. The separatrices are shown by thick lines. The isolines are drawn with a velocity step of 0.005 for the top layer and 0.01 for the bottom layer. The cross marks the rotation centre, coinciding with the central vortex of the top layer. The closed dashed line is the trajectory of the bottom-layer particle with minimum turnover frequency. (*b*) Dependences of turnover frequency $\Omega(x_0)$ (solid lines) and azimuthal velocities $v(x_0)$ (short-dash lines) of fluid particles originating from the x-axis, as functions of the distance x_0 from the origin of coordinates. Insets with extended vertical coordinates demonstrate the behaviour of curves in critical domains. Long-dash straight lines show asymptotes corresponding to solid-body rotation with an angular velocity given by (3.1) in SKV.

bottom-layer vortices. The separatrix in the top layer has a heteroclinic structure. A heteroclinic separatrix, embracing the point vortices, forms in the bottom layer. The dashed streamline in the bottom layer corresponds to a minimum of the turnover frequency. The dependence on the initial position taken on the axis $y = 0$ for turnover frequency Ω and on the azimuthal velocity v of fluid particles are also given here. Because of symmetry, only the right part of the figure is given (for positive abscissa). Within the separatrix, in the vicinity of point vortices, we have indefinitely growing turnover frequency and azimuthal velocity, which corresponds to the singularity in point vortices. The situation beyond the separatrix is also of great interest. The turnover frequency has a maximum near the separatrix and a minimum at a considerable distance from it (the inset in the bottom figure), while the

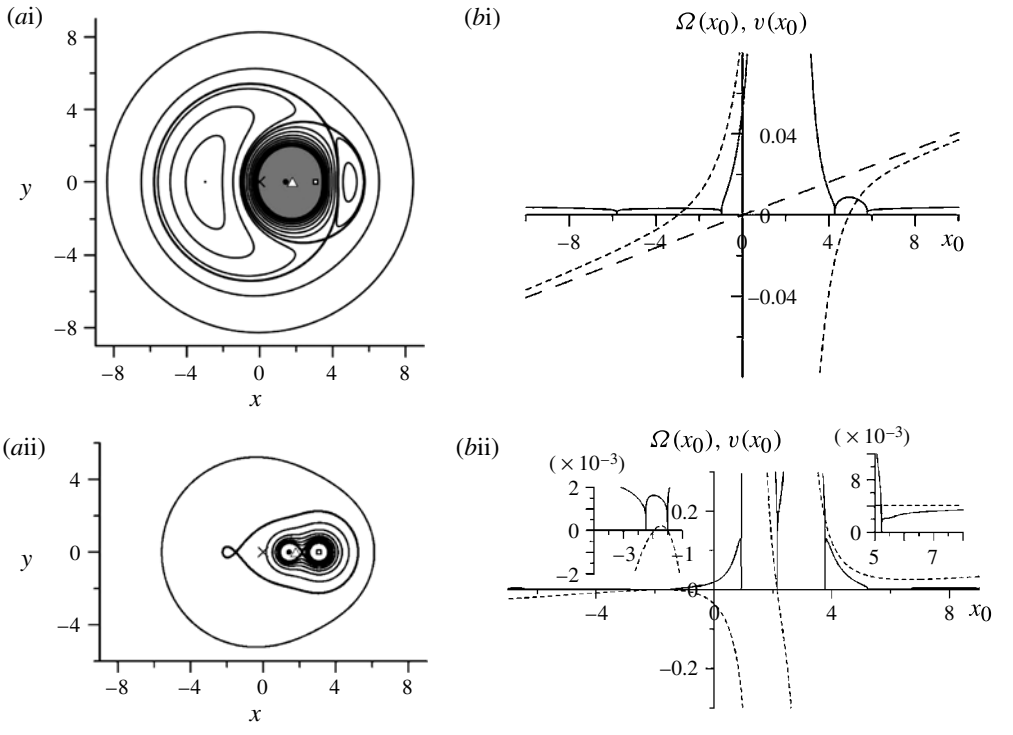

FIGURE 3. The same as in figure 2, but with $B = 0.3712$, $R = 0.8200$. The isolines are drawn with a step of 0.010 for the top layer and 0.025 for the bottom layer.

velocity of particles has only a minimum, which is somewhat closer to the centre than the frequency minimum. The behaviour of the velocity and turnover frequency with distance from the centre corresponds to a solid-body rotation of the roundabout (the fluid is motionless at infinity in the absolute coordinate system).

Figure 3(*a*) gives phase portraits for both layers for the ($R = 0.8200$, $B = 0.3712$) situation, which appreciably differs from symmetry. The left loop of the outer separatrix in the top layer has increased due to the effect of rotation of the vortex system as a whole, and the turnover frequency of particles along the trajectory in this loop has dramatically decreased. In the bottom layer, the separatrix embracing the point vortices is now asymmetric (its left loop has decreased), and an additional external asymmetric heteroclinic separatrix, containing the internal separatrix in its large right loop, has formed. In the external domain, the fluid is still asymptotically motionless.

The patterns of streamlines for the case $R = 1.5$ for small distance between the vortices $\binom{1}{1}$ and $\binom{1}{2}$ are given in figure 4 where $B = 0.0246$. In this case, domains of closed motion of fluid particles (induced vortices), separated from the separatrix by a domain of another closed current, form in the bottom layer above and below the main separatrix. The vorticity centre now lies at a greater distance from the vortex structure and outside the internal separatrix. Now the external separatrix can be interpreted as a homoclinic structure with connected 'whiskers', and in phase portraits, the vicinity of the roundabout can be isolated in both layers, moving along separatrix whiskers

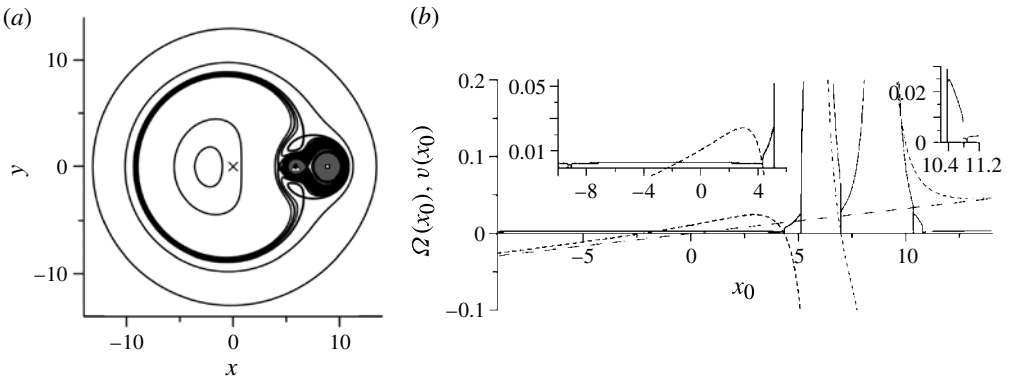

FIGURE 4. The same as in figure 2, but with $B = 0.0246$, $R = 1.5000$. Only the bottom layer is shown. Isolines are drawn with a step of 0.001.

which encompass the rotation centre. The situation in the top layer shows almost no qualitative changes.

In frequency relationships, the boundary of the closed flow can be clearly seen in figure 4(*b*) in insets near the values $x_0 = -9$ and $x_0 = 11$. Note that a closed flow, separating the internal and external separatrices still persists in this case. This flow is also identified based on the frequency relationship, and, as can be clearly seen in the inset, these two flows are separated by the external separatrix.

Consider an important particular case corresponding to a *reconnection* of the separatrix of induced vortices with the external separatrix of a roundabout. This situation is shown in figure 5. The two separatrices have merged here and the domain of the external closed flow has disappeared. In such situations, under a perturbation of a stationary configuration, it is very likely that a wide chaotic domain will appear in the vicinity of such a merged separatrix (Koshel *et al.* 2008; Sokolovskiy, Koshel & Carton 2010). Unlike the situation in figure 4(*b*), there is no domain of external closed flow for frequency relationships, which we do not give here. No significant changes are observed in the top layer either; therefore, we simply show the separatrices of the top layer, superimposed on the phase portrait of the bottom layer. The comparison of separatrix configurations gives an idea of the shape of the fluid column captured by the roundabout, and allows us to conclude that when R is large enough, this column is localized in the rectangular box drawn in figure 5.

2.2. *Dependence on* μ

To analyse the effect of parameter μ on the character of phase portraits of an eccentric roundabout, we consider a series of dispersion curves (the solutions to (3.2) and (3.6) in SKV) with different μ (figure 6). They are qualitatively similar to one another with the limiting value $R_0^{(r)}$ increasing from zero at $\mu = -\infty$ to infinity at $\mu = -1$, when $B = R$. Curves X_c are also plotted here, displaced by the value of B for all given values μ except $\mu = -2$ (triton) when $|X_c| = \infty$.

Calculations show that the topological properties of phase portraits, shown in figures 2–5 for the case $\mu = -2.5$, may also appear at other values of parameter μ. However, because of the special role of the value $\mu = -2$, the crossing of this level is accompanied by changes in the phase picture which are illustrated in figure 7 by two examples with $\mu < -2$ and $\mu > -2$. Thus, when $\mu = -4$ (figure 7*a*), the structure

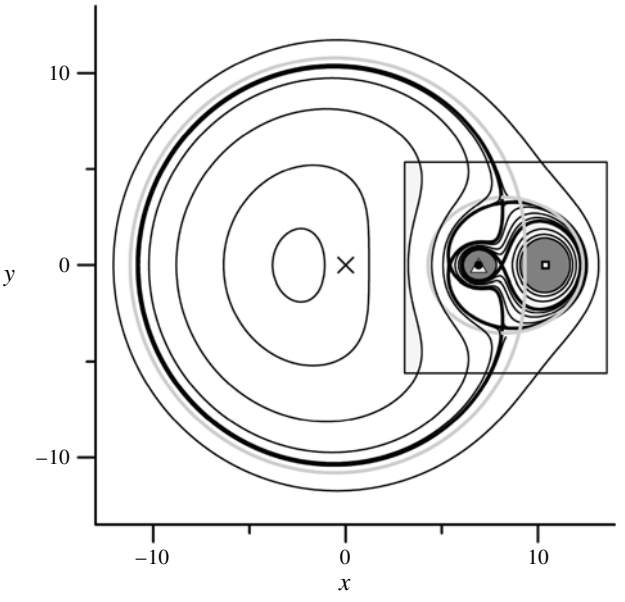

FIGURE 5. Isolines of the stream-function in a co-rotated coordinate system with $B = 0.0119$, $R = 1.7418$ and $\mu = -2.5$. Streamlines with a step of 0.005 are given only for the bottom layer. The grey lines show top-layer separatrices. The structure of the boxed domain will be described in the text.

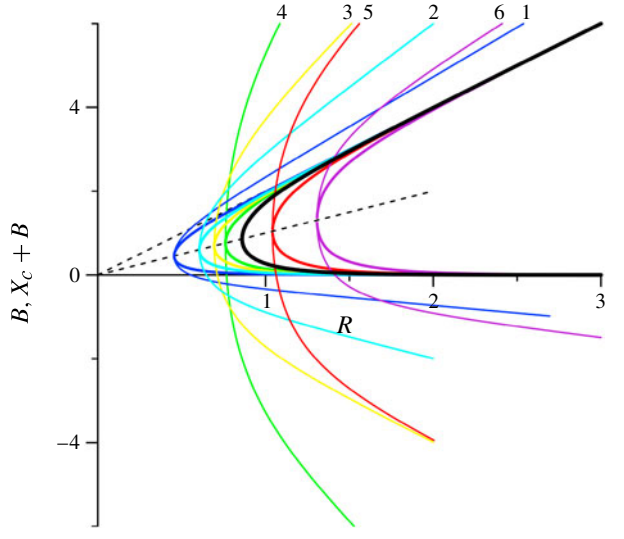

FIGURE 6. Dispersion curves $B(R)$ (within the angle between the straight lines $B = 0$ and $B = 2R$) and dependence $[X_c + B](R)$ for an eccentric roundabout with: **1**, $\mu = -7.5$ (dark blue); **2**, $\mu = -4.0$ (light blue); **3**, $\mu = -3.0$ (yellow); **4**, $\mu = -2.5$ (green); **5**, $\mu = -1.5$ (red); **6**, $\mu = -1.2$ (magenta). The curve corresponding to the triton at $\mu = -2.0$ is marked by a black line. The inclined dashed line $B = R$ is the axis of symmetry of curves given by (3.2) and (3.6) in SKV, while the line $B = 2R$ and the axis R are their asymptotics at $R \gg 1$.

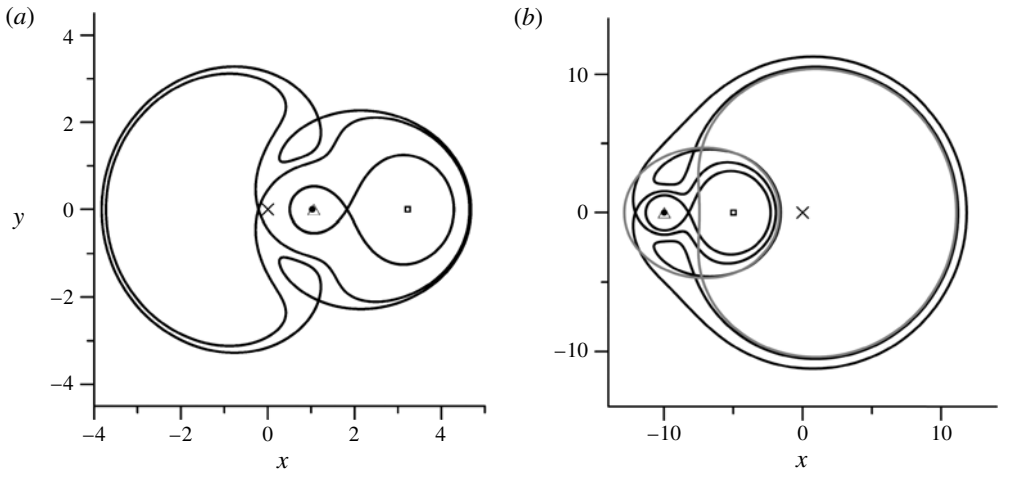

FIGURE 7. Separatrices of the stream-function field in the bottom layer in a coordinate system rotating with the angular velocity (3.2) in SKV: (*a*) $R = 1.1$, $\mu = -4.0$; and (*b*) $R = 2.5$, $\mu = -1.5$. In (*b*), for comparison, the grey line is the separatrix in the top layer.

of separatrices in the bottom layer is the same as with $\mu = -2.5$ (figure 2), and the only difference is that now the rotation centre is localized outside the left loop of the inner separatrix. However, when $\mu = -1.5$ (figure 7*b*), the rotation centre moves to the right half-plane, the motion of the vortex structure changes its direction, and the vortex atmosphere, surrounding the point vortices, appears within the loop composed of separatrix whiskers, embracing the rotation centre.

2.3. *Triton case*

The further analysis of bifurcations of phase portraits will be based on the case of a triton ($\mu = -2$). There is no large difference in the most important part of the phase portraits, as will be shown below. Only the limiting case $B = R = R_0^{(r)}$ has some difference due to the infinite character of triton motion.

As before, we begin with the limiting symmetrical state $B = R = R_0^{(r)} = 0.8602$, which in this case is static. Figure 8(*a*) gives phase portraits and figure 8(*b*) gives frequency characteristics of fluid-particle motion. The latter, by virtue of symmetry, are given only for positive values of the initial positions along the axis x or y. In particular, the top panel and the inset in figure 8(2*b*) shows the dependence of the turnover frequency on the coordinate y_0 in the vicinity of the top elliptic point located above the branch of the quasi-separatrix for the bottom layer (this branch runs to infinity), where such frequencies are much lower than in the top layer.

It is significant that the turnover frequencies outside the separatrices embracing point vortices are much lower than inside these separatrices. In induced vortices (separated from point vortices by two separatrices), the frequencies are also much less, a fact that will play a significant role in the analysis of possible chaotic regimes after perturbation of steady solutions. In the same figure, dashed lines show the behaviour of azimuthal velocities of fluid particles that have started from appropriate coordinate axes.

As before, we will consider pairs of values B and R, referring to the lower branch of the curve in figure 5 in SKV. Here, $B \leqslant R$, the triton's velocity is negative, and the

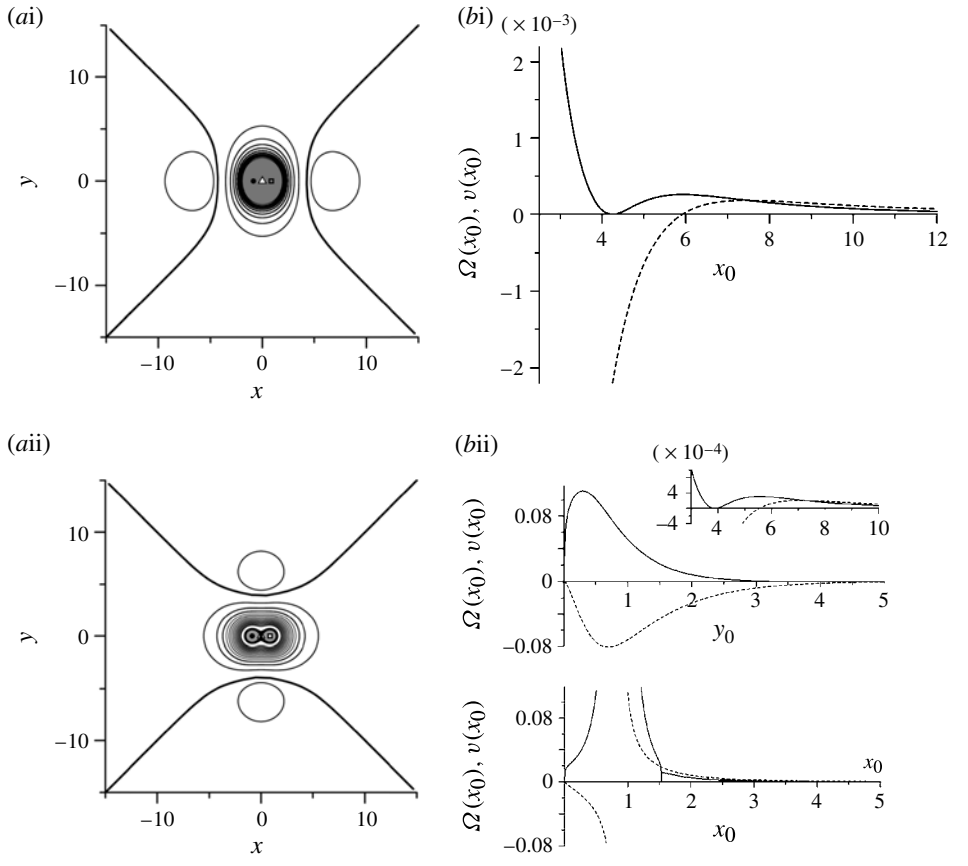

FIGURE 8. (*a*) Isolines of the stream-function in a fixed coordinate system with $B = R = R_0^{(r)} = 0.8602$ (static position) in the top (i) and bottom (ii) layers. Separatrices are shown by thick lines. Isolines are drawn with a step of 0.005 for the top layer and 0.01 for the bottom. (*b*) Turnover frequencies Ω (solid lines) and azimuthal velocities v (short-dash lines) of fluid particles that have started from the x- or y-axes as functions of distance x_0 or y_0 to the origin of coordinates. Insets with extended vertical coordinates elucidate the behaviour of curves in critical domains.

vortex structure in the figure moves downward. In the coordinate system moving with the triton, the slip flow is directed upward.

Figure 9 shows the near-limiting case of $R = 0.8602$. Even with the deviation from the symmetrical position of vortices as small as that, considerable deformation takes place in the phase portrait. The separatrices of induced vortices take the classical homoclinic form. In the top layer, the left induced vortex detaches from the main separatrix, while the two vortex domains on the right are joined by a common separatrix. Three isolated vortex domains form in the lower layer. An interesting feature is the appearance of two narrow zones of flow-through currents in the bottom layer and one such zone in the top layer, where the separatrices of induced vortices closely approach the main separatrices. Though the velocities of fluid particles are not large here, they are still far in excess of the velocity of the triton itself. These zones can be associated with the jet flows generated by the triton.

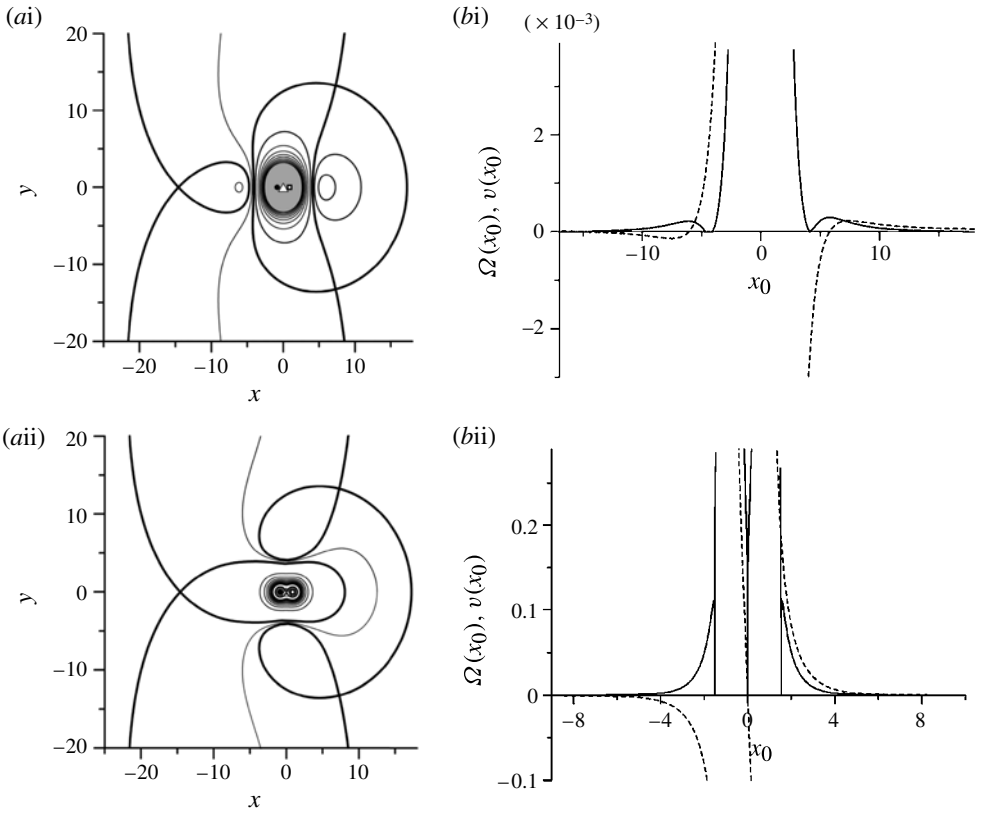

FIGURE 9. (*a*) The same as in figure 8, but in a coordinate system moving translationally with a velocity given by (3.7) in SKV at $\mu = -2$, $R = 0.8602$, $B = 0.8565$. The isolines are drawn with a step of 0.002 for the top layer, (i), and with a step of 0.01 for the bottom, (ii). (*b*) Dependences (on the distance x_0 to the origin of coordinates) of turnover frequencies Ω (solid lines) and azimuthal velocities v (short-dash lines) of fluid particles that have started from the x-axis.

With a further increase in R, the induced vortex domains, not associated with point vortices, degrade and then disappear completely, this process finishing earlier in the top layer than in the bottom. This effect is illustrated by figure 10(*a*,*b*), showing examples of phase portraits for the top and bottom layers, respectively, with those (different!) values of R and B, for which the left domain of closed circulation disappears in the top layer and the two vortex domains disappear in the bottom layer. The appropriate separatrix, clearly, also disappears. It is obvious that the jet flow domains are also not pronounced here.

The subsequent increase in the asymmetry of a triton caused by an increase in parameter R within a wide interval does not cause qualitative changes in phase portraits, though, as can be seen from figure 11, evolutionary changes in the picture take place. With this set of external parameters, the effect of vortex structure on the background flow is more significant in the left part of the domain in the top layer and in its right part in the bottom layer. The frequency dependences for this configuration will be analysed in the following section.

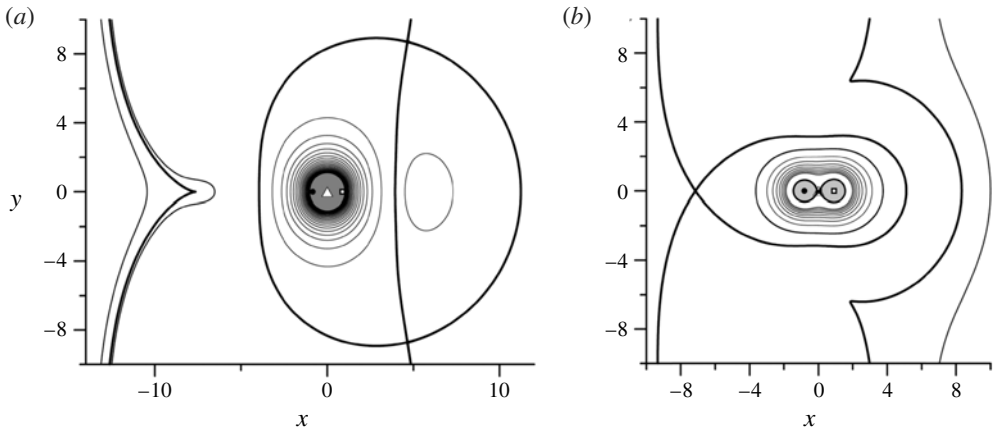

FIGURE 10. Isolines of the stream-function in a fixed coordinate system with $\mu = -2$ and (*a*) $R = 0.86023$, $B = 0.8458$ (top layer) and (*b*) $R = 0.86050$, $B = 0.8234$ (bottom layer).

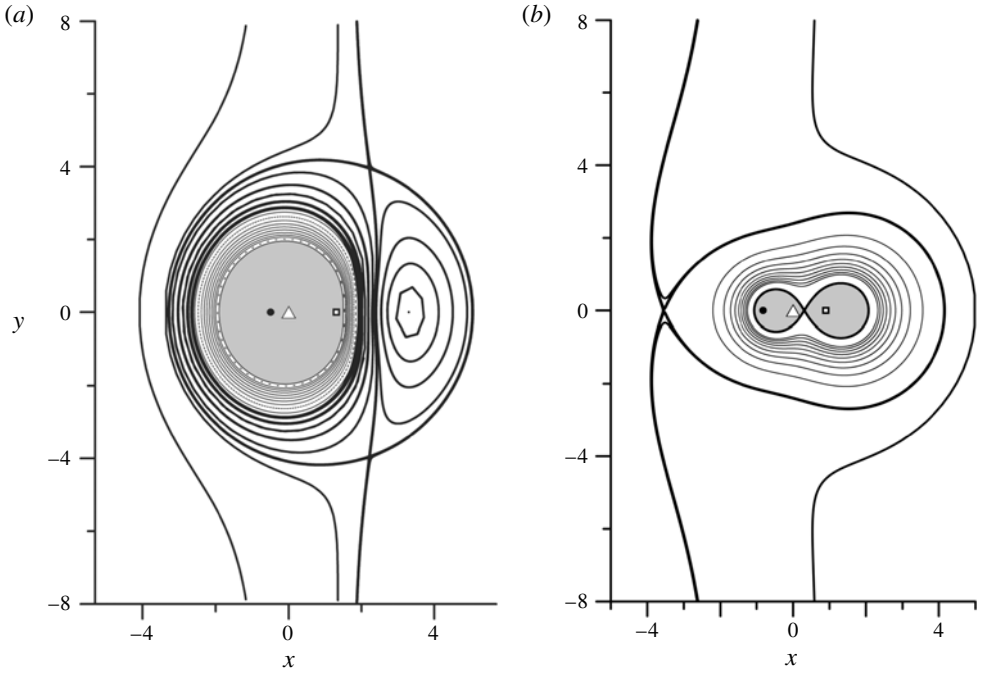

FIGURE 11. Isolines of the stream-function at $\mu = -2$ and $R = 0.90$, $B = 0.4923$ with a step of 0.005 in the top layer (*a*) and 0.01 in the bottom layer (*b*).

As R grows further, the structure of the stream-function field in the top layer shows practically no changes, so we will consider a number of phase portraits only for the bottom layer (figure 12), demonstrating a series of new bifurcations.

In figure 12(*a*,*b*), we essentially observe the process of revival of the separatrix that had disappeared before and the formation of new finite domains of motion of fluid

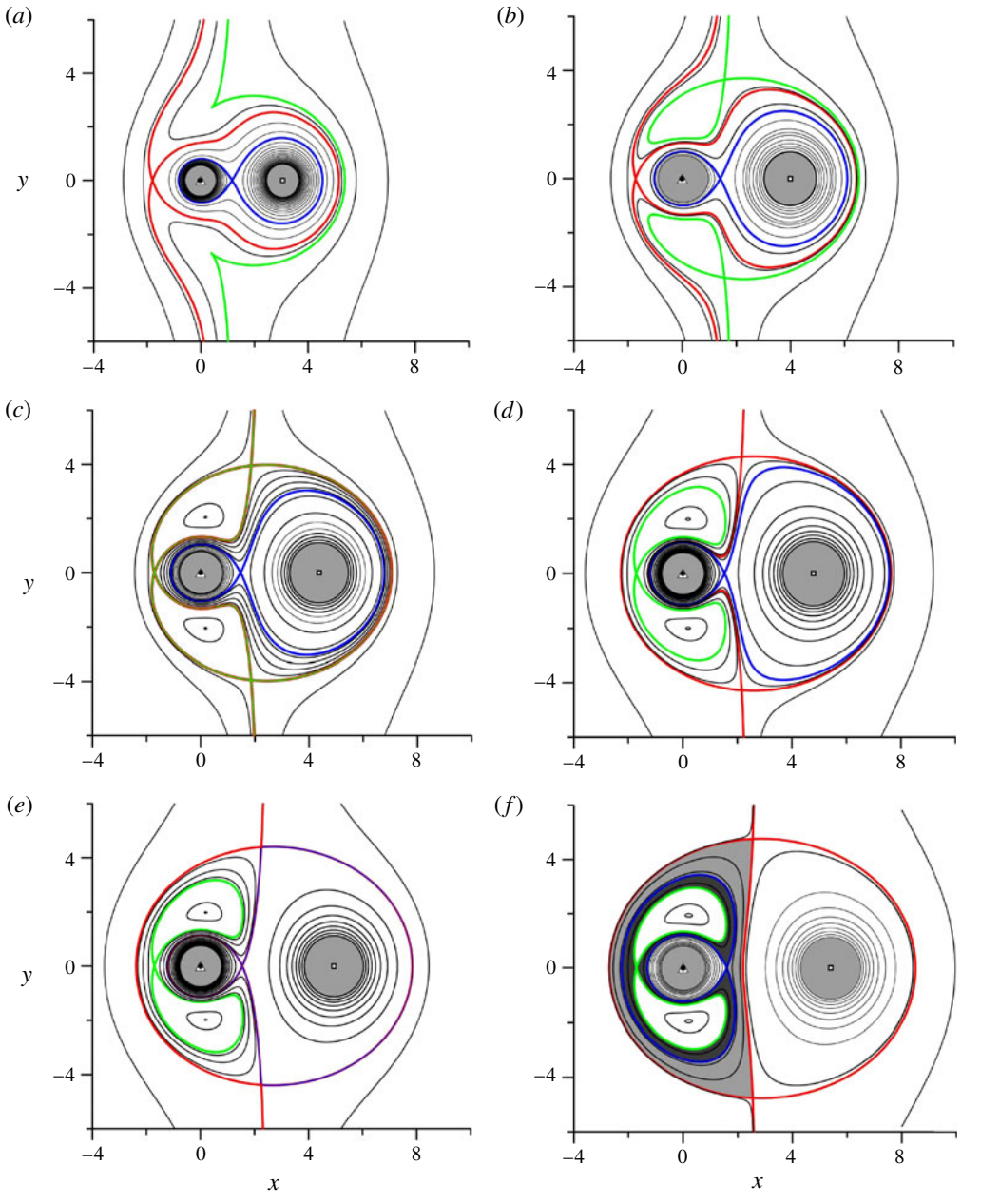

FIGURE 12. Isolines of the stream-function in the bottom layer at $\mu = -2$ and the following another parameter values: (*a*) $R = 1.546$, $B = 0.03523$, $V = -0.01750$; (*b*) $R = 2.0$, $B = 0.009255$, $V = -0.01699$; (*c*) $R = 2.1881$, $B = 0.005516$, $V = -0.01628$; (*d*) $R = 2.4$, $B = 0.003131$, $V = -0.01539$; (*e*) $R = 2.470$, $B = 0.002608$, $V = -0.01412$; (*f*) $R = 2.70$, $B = 0.001438$, $V = -0.01200$. Here, V is the triton velocity (formula (3.7) in SKV).

particles, tending to a two-layer, practically vertical, vortex structure, consisting of an anticyclone in the top layer and a left-hand cyclone in the bottom layer. The new separatrix in figure 12(*b*) to a considerable extent embraces the external separatrix of

the entire vortex structure, while in figure 12(*c*), we observe their *reconnection*, at which they completely merge and acquire heteroclinic character. Next (figure 12*d*), these separatrices split at the left hyperbolic point, and the green line now becomes a boundary of a two-cell domain of closed motions of particles. The next reconnection phenomenon can be seen in figure 12(*e*). Here, the blue heteroclinic structure merges with the external (red) separatrix, while the right loop disappears and the left one becomes a homoclinic structure. Fluid exchange between the left, tripolar, and the right, monopolar, domains ceases. Next, in figure 12(*f*), we again see the splitting of separatrices, after which the blue separatrix, remaining homoclinic, separates from the red one, while its whiskers close on the green separatrix. In this figure, two domains of closed regular flows in the domains separated by separatrices in the left loop are shown by grey shading with different intensities.

The volume of the atmosphere of the vortex structure associated with the red separatrix steadily increases with an increase in parameter R (from figure 12*a* to 12*f*). In general, a characteristic feature of the baroclinic model is the non-monotonic dependence of the size of the vortex atmosphere of the triton on parameter R, as well as its translational velocity. We think it is impossible to exactly evaluate the mean radius of the atmosphere, but calculations show its minimal size to lie nearly in the same interval of R values where the triton's velocity is maximal.

Note that the picture of advection in the vicinities of the triton and the roundabout are similar: compare, for example, figure 12(*c*) and the domain enclosed by the square in figure 5. Moreover, the bifurcation features of the phase portraits also have appropriate analogues in these two cases. This also points to the non-monotonic character of behaviour of the mean radius of the atmosphere surrounding it. The main distinction is that the whiskers running to infinity in the triton are closed in the roundabout.

No new bifurcations are observed during the subsequent increase in R, and it is only in the limit $R \to \infty$ that a reconnection of the green and blue separatrices takes place, accompanied by their degeneration with a tendency to acquire a generally circular shape. These effects are demonstrated by figure 13, where $R = 10$. It is evident that the size of the vortex atmosphere here has increased appreciably.

An important point is the localized character of singularities. In the majority of vortex domains adjacent to the external separatrix, the azimuthal velocity and frequency are relatively small (see figure 13). Because of this, we can expect that sufficiently pronounced chaos-inducing effects will appear for small perturbations of the stationary construction. On the other hand, the domains with a small derivative of the frequency with respect to x_0, i.e. with a small nonlinearity parameter, can serve as barriers for chaotic advection, i.e. separate the well-mixed domain around the centres of singular vortices from the domain of chaotic transport in the vicinity of the separatrix. In the following section, we consider some mechanisms of origination of chaos in the context of this problem.

3. Examples of the behaviour of fluid particles in the velocity field of a perturbed triton: chaotic advection

In previous sections and SKV, we considered the motion of a system of vortices in both stationary and non-stationary cases and evaluated the characteristic frequencies of perturbed motion. The perturbed stationary configurations were shown either to move translationally with a constant mean velocity or to rotate about a centre of rotation with a constant mean angular velocity. Thus, passing to a coordinate system moving

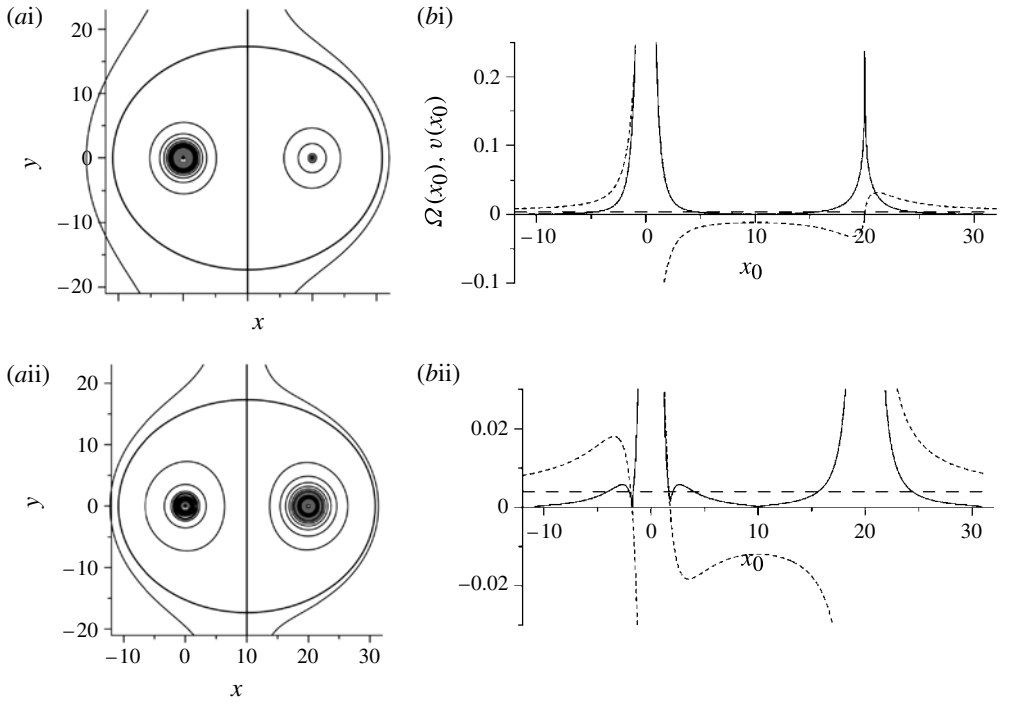

FIGURE 13. (*a*) Phase portraits and (*b*) turnover frequencies Ω (solid lines) and azimuthal velocities v (short-dash lines) of fluid particles at $R = 10.00$ and $B = 0.0000000046$. The isolines are drawn with a step of 0.01 for both layers: (i) the top layer, (ii) the bottom layer. Notation is the same as in figure 8.

with appropriate translational or angular velocity, we can study the non-stationary motion of a system of vortices in the vicinity of some averaged stationary state. Under small perturbations, the motion of fluid particles will be close to the motion in a velocity field induced by a stationary mean state of the vortex system (such motion was considered in the previous section). In the perturbed case, the induced velocity field will be non-stationary but periodic, with a period of relative motion. In this situation, the so-called *separatrix chaos* can appear in the *stochastic layer* (a narrow domain in the vicinity of the separatrix of an induced velocity field). With larger perturbations and appropriate choice of perturbation frequencies, the separatrix chaos can transform into *global chaos* or, in other words, into a *stochastic sea* (Zaslavsky 2007).

As shown above for a non-perturbed case, a considerable number of fluid particles have characteristic turnover frequencies comparable with the frequency of relative motions (the frequency of non-stationary perturbation). In this case, it is very likely that chaotic motion will appear in domains remote from separatrices because nonlinear resonance domains overlap (Zaslavsky 2007; Koshel *et al.* 2008). Barriers consisting of regular trajectories (KAM-tori) may exist between the domains of separatrix chaos and the domains of overlapping of large-scale nonlinear resonances. These barriers can be destroyed without an increase in perturbation amplitude only because of a successful choice of the frequency at which reconnection of separatrices takes place.

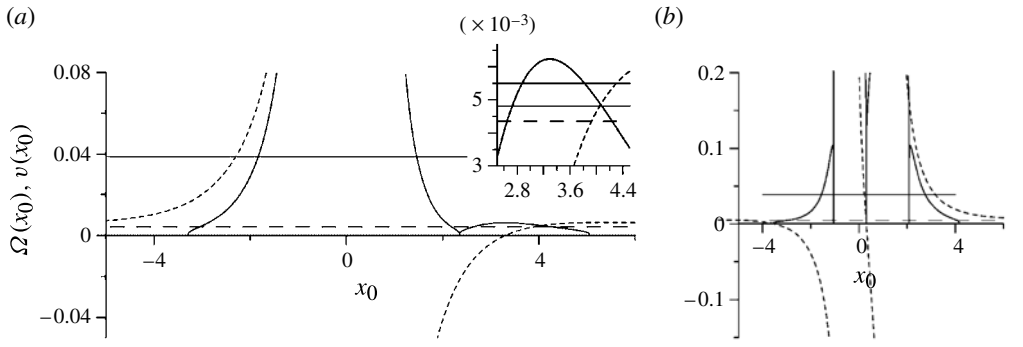

FIGURE 14. Dependences of turnover frequencies Ω (solid lines) and azimuthal velocities v (short-dash lines) of fluid particles on their initial position on the x-axis for the top (a) and bottom (b) layers. The long-dash horizontal line is triton velocity. The solid horizontal lines in (a) and (b) show the frequency $\tilde{\omega}$ of perturbed motion. The solid horizontal lines in the inset show $\tilde{\omega}/8$ and $\tilde{\omega}/7$ of the perturbed motion frequency. The curves correspond to the phase portrait of figure 11 where $\mu = -2$ and $R = 0.90$, $B = 0.4923$.

Below, we will consider three examples of perturbed configurations, illustrating the global separatrix chaos and the destruction of a regular barrier for chaotic transport through reconnection of separatrices. We will limit our consideration to the case of a perturbed triton, since the formation of chaotic regions in the case of an eccentric roundabout is analogous.

For simplification, we will consider perturbations preserving the zero component of the impulse P_y. We can consider the class of initial configurations with symmetric displacement of the peripheral vortices in the bottom layer, i.e. replace R by $R + \Delta R$ and B by $B + \Delta R$.

Let us return to figure 11, exemplifying streamlines for the motion of fluid particles in a velocity field induced by a triton, at $R = 0.90$, $B = 0.4923$. As shown in the studies by Izrailsky *et al.* (2006, 2008) and Koshel *et al.* (2008), to reach maximal degree of chaotic behaviour of trajectories in the vortex domain requires that the turnover frequencies of non-perturbed trajectories and the frequencies of non-stationary perturbation are of the same order.

In the case under consideration, the perturbation frequency can be estimated by formula (4.24) in SKV, yielding $\tilde{\omega} \approx 0.0385$. To construct a possible scenario of transition to chaos of trajectories we need to know the turnover frequencies of fluid particles in the vortex domain in the absence of perturbation. The appropriate dependences on the initial position x_0 of a particle on the x-axis are given in figure 14. The solid horizontal line shows the frequency of the perturbed motion. We can see that the perturbation frequency and the turnover frequencies in the top and bottom layers are of the same order of magnitude in a considerable portion of the vortex domain.

The intersection of the horizontal line in figure 14, indicating the perturbed motion frequency, with the plot of turnover frequency of fluid particles shows the trajectory on which the 1:1 nonlinear resonance takes place. As a rule, this is the largest resonance in the system. Maximal chaotic area can be expected to occur in the vicinity of such a trajectory.

Figure 15 gives the corresponding Poincaré sections. To begin, we consider the top layer (figure 15*a*). In the vortex domain containing the central vortex, the intersection takes place at the initial coordinates of $x_0 \approx -2.0$ and $x_0 \approx 1.5$. The Poincaré sections

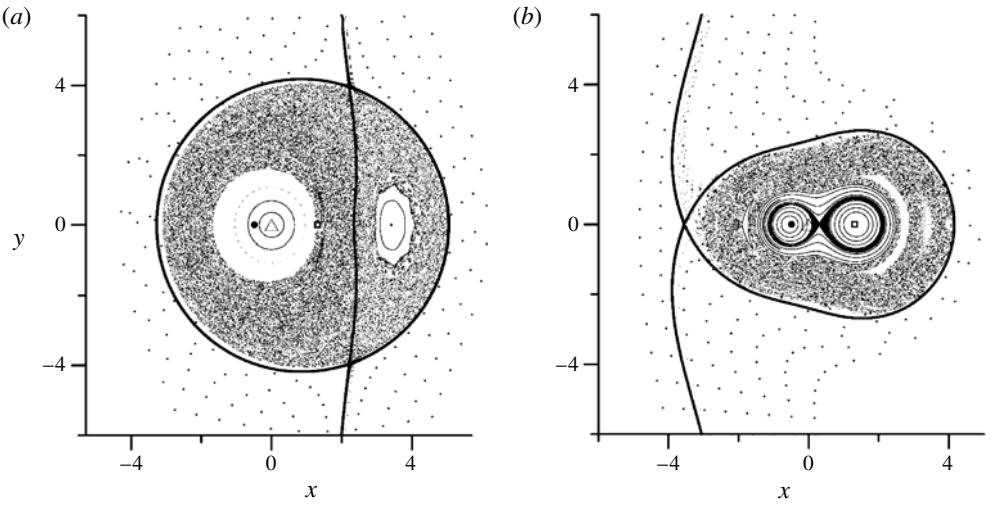

FIGURE 15. Poincaré sections for a perturbed triton at $\mu = -2$, $B = 0.4923$, $R = 0.9$ and $\Delta R = 0.05$ for the top (a) and bottom (b) layers. The phase portrait for a non-perturbed case is shown in figure 11.

in this example correspond to the external problem in the terminology of Kozlov & Koshel (2001) and have been calculated in the following manner: 11 markers were placed within the segment $[-2.0 < x_0 < 4.0, y_0 = -6]$ and 11 more markers were placed in a small segment in the vicinity of the separatrix at $y_0 = -6$; the positions of these markers were output once during each period of perturbation. The behaviour of markers that were initially located far from the separatrix is of regular character: they move around the vortex domain in almost the same manner as unperturbed trajectories. The markers that were placed near the separatrix can penetrate into the vortex domain, demonstrating features of fractal behaviour: some penetrate into the vortex domain, while others do not. The markers that have penetrated into the vortex domain demonstrate chaotic behaviour within the separatrix, and a boundary of the chaotic domain can be clearly seen in the left part of the vortex domain. This boundary corresponds to the position of the 1:1 resonance, i.e. $x_0 \approx -2.0$, which corresponds to a hyperbolic point of nonlinear resonance, and $x_0 \approx 1.5$, which is smaller than the position of the non-perturbed resonance trajectory by the width of the resonance domain. The situation is somewhat more complicated in the right part of the vortex domain, which is subject to the effect of the right vortex of the bottom layer. In the frequency dependence for this domain, we see that 1:1 resonance cannot take place.

The inset in figure 14 shows the levels corresponding to frequencies $\tilde{\omega}/7$ and $\tilde{\omega}/8$. The largest feasible resonance has the ratio of 1:7 and consists of seven islands; i.e. there are seven elliptic and seven hyperbolic points. The domains of resonances 1:7 and 1:8 have a smaller width than the 1:1 resonance; therefore, the boundary of the chaotic zone lies further from the elliptic point of the right vortex domain. The analysis of the shape of this boundary shows it to lie between the domains of resonances 1:7 and 1:8, i.e. we see partial overlapping of these resonances.

The situation in the bottom layer is radically different (figure 15b). First, because of the singularity and the point vortices belonging to this layer, the turnover frequency

of fluid particles very rapidly decreases in the vicinity of the internal separatrix, embracing the point vortices. The second significant distinction is that the external vortex domain has no elliptic point and is located between two separatrices. Since the turnover frequency vanishes on separatrices, there exists a trajectory between them, corresponding to a maximum of turnover frequency.

The two intersections of the curve of turnover frequency and the horizontal line corresponding to the perturbation frequency lie on two different trajectories. Note that the two symmetric domains with turnover frequency maxima with negative and positive x_0 correspond to the same trajectories; therefore, it is sufficient to consider only one of these domains. The problem in which closed streamlines lie between separatrices and the frequency dependence has a single maximum has been considered in detail in Koshel *et al.* (2008), where one of the separatrices was at infinity. Such a situation admits the existence of two sets of nonlinear resonances with the same multiplicity and, accordingly, reconnections of separatrices of these resonances are possible. Without going into detail, we note that the model demonstrates all effects revealed in the above-cited paper.

Thus, in the lower layer, the curve of turnover frequency intersects with the level of perturbation frequency very close to the separatrix, in both the internal and external vortex domains; hence, we have a very narrow separatrix stochastic layer. One more non-trivial intersection takes place in the external vortex domain on the trajectory passing through points $(x_0 \approx -1.55, y_0 = 0)$ and $(x_0 \approx 2.75, y_0 = 0)$.

As a result, we have an island of regular behaviour corresponding to the 1:1 resonance at $x_0 \approx 2.75$, and the boundary of the stochastic sea passes through points $(x_0 \approx -1.52, y_0 = 0)$ and $(x_0 \approx 2.55, y_0 = 0)$, i.e. it is separated from the position of the resonance trajectory by the width of the resonance domain. Moreover, we see a partially destroyed 1:2 resonance consisting of two islands of regular behaviour, therefore these two largest nonlinear resonances in this case also partially overlap.

The degree of chaos in the external domain will be appreciable, the perturbation of the triton being relatively small; in other words, the perturbation is not large for the triton, but sufficiently large from the viewpoint of the approaching nonlinear resonance. The stochastic layer in the vicinity of the internal separatrix is very narrow, since, because of singularity, the derivative of frequency with respect to the initial position of the trajectory is very large in this domain and hence, the thickness of the stochastic layer is very small here. Because of the singularity, vicinities of point vortices should be regular (Ryzhov & Koshel 2010). Thus, the internal separatrix and the external chaotic domain are separated by a barrier hampering the transport of fluid particles from the central part of the vortex atmosphere to its periphery.

An important point is the capture and release of part of its mass by the vortex atmosphere. The capture of fluid from the incoming flow is possible only within a very narrow domain near the separatrix. The release of fluid particles also takes place in a narrow domain near the separatrix on the opposite side of the vortex atmosphere. Tentative estimates show that, on the one hand, this is a very slow process, but, on the other hand, all the fluid in the external chaotic domain will be, sooner or later, carried out from the vortex atmosphere.

Figure 16 gives an example where the degree of chaotization is relatively small in the bottom layer and considerable in the top one. These differences were obtained by the choice of a sufficiently small perturbation amplitude, corresponding to high-frequency perturbed oscillations.

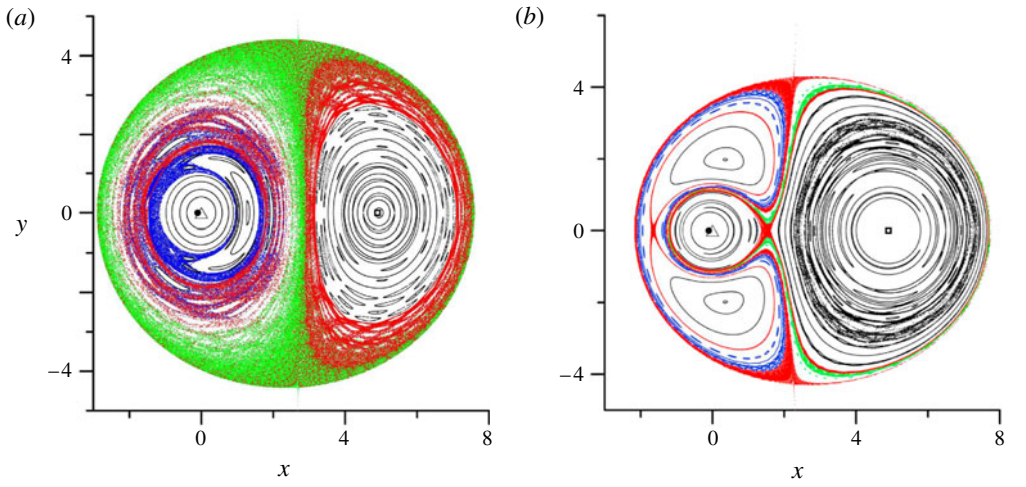

FIGURE 16. Poincaré sections at $\mu = -2$, $B = 0.003131$, $R = 2.4$ and $\Delta R = 0.1$ for the top (a) and bottom (b) layers. The figures correspond to perturbed behaviour of the triton, whose non-disturbed phase portrait is given in figure 12(d), and separately, the separatrix shown in figure 19(a).

However, the effect is largely governed by the dependence type of the turnover frequency of fluid particles in the velocity field induced by a stationary configuration. In studies by Izrailsky *et al.* (2006, 2008), Koshel *et al.* (2008) and Ryzhov & Koshel (2010), it is shown that when perturbations are not too small, the formation of chaotic regions in phase portrait domains not adjacent to separatrices can be characterized by the overlapping degree of nonlinear resonances, which, in its turn, is largely determined by the width of the resonance domains and the distance between neighbouring resonance domains. These parameters are determined by the derivative of the turnover frequency with respect to action, which is proportional to the derivative of the frequency with respect to coordinate.

Consider figures 16 and 18 from this viewpoint. Figure 18 shows the frequency levels $\tilde{\omega}/n$ corresponding to a series of largest resonances. Here we see all four types of frequency dependence, introduced in Ryzhov & Koshel (2010). The first one is a phase portrait with a singular point and a small distance to the separatrix; two such areas are realized in the lower layer. As shown in this work, in the vicinity of the singular point, the trajectories regularize even for very large perturbations; so, in the lower layer the chaotic area is pressed against the separatrix. The second type is an area with a regular elliptic singular point only a short distance from the separatrix. This type is realized in small areas of induced recirculation. In this case, it is possible that the vortex area becomes completely chaotic, if the perturbation frequency is comparable to the turnover frequency in the vicinity of the elliptic point. Figure 18 shows the maximum turnover frequency of the induced vortex areas to be far less than the perturbation frequency in this case, and accordingly, we have here a narrow stochastic layer along the separatrices, since the Chirikov criterion starts to apply near the separatrix (Chirikov 1979; Zaslavsky 2007; Koshel *et al.* 2008) for the high-order resonances.

The next type of phase portrait corresponds to the singular critical point and large distance from it to the separatrix. Between the area of regularization near the singular point and the separatrix there exists an area with an action derivative of the frequency

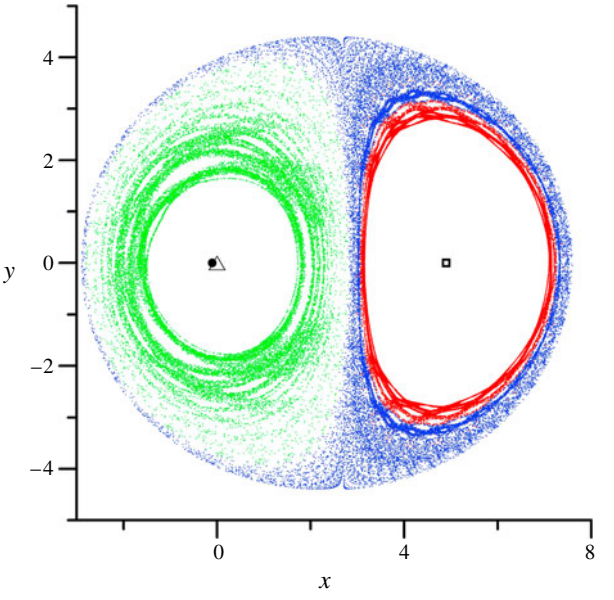

FIGURE 17. Three-colour illustration of the trap effect of the red marker in the top layer (figure 16*a*). Here, red markers correspond to the first 40 000 perturbation periods, blue markers to the next 20 000 periods, and green markers to the next 20 000 periods. See details in the text.

of the order of unity, and the frequency of the perturbation is comparable to the turnover frequency in this area. In this case, we have a stochastic sea from the boundary of the regularization area ($x_0 = 1.7, y_0 = 0$) to the separatrix. In addition, in the vicinity of the trajectories with initial positions near ($x_0 = 2.0, y_0 = 0$), we can see in figure 16(*a*) a semipermeable barrier (a cantor), because the nonlinearity parameter is minimal in this narrow region. This leads to the fact that markers (shown in blue) remain for a long time in the vicinity of the boundary of the regularization area, and markers from the vicinity of the separatrix (green and red) penetrate very slowly into this area.

The last type represents a domain with a regular elliptic point and a large distance from it to the separatrix. This type of phase portrait occurs in the induced (right) vortex area of the upper layer. Here, however, the maximum turnover frequency in the vicinity of an elliptic point is very large, and the amplitude of a non-stationary perturbation, as seen in figure 16(*a*), is insufficient to meet the Chirikov criterion (resonance overlapping). Thereby, in this area, we see a wide stochastic layer near the separatrix or the initial stage of the transition to the stochastic sea. The distinction of this area from the left singular one consists in the fact that there is no regularization in the vicinity of an elliptic point. So, if the perturbation amplitude is increasing, the stochastic sea may extend up to the elliptic point. This becomes evident due to the beginning of the partial destruction of the nonlinear resonance separatrices in this area, indicated by black markers. The degree of overlap of nonlinear resonances increases with the approach to the separatrix. Therefore we have semipermeable barriers near the boundary of the stochastic layer, similar to the barrier in the left panel.

The effect of traps is more vividly illustrated by figure 17, which shows the behaviour of the particle marked by red in figure 16, though three colours are

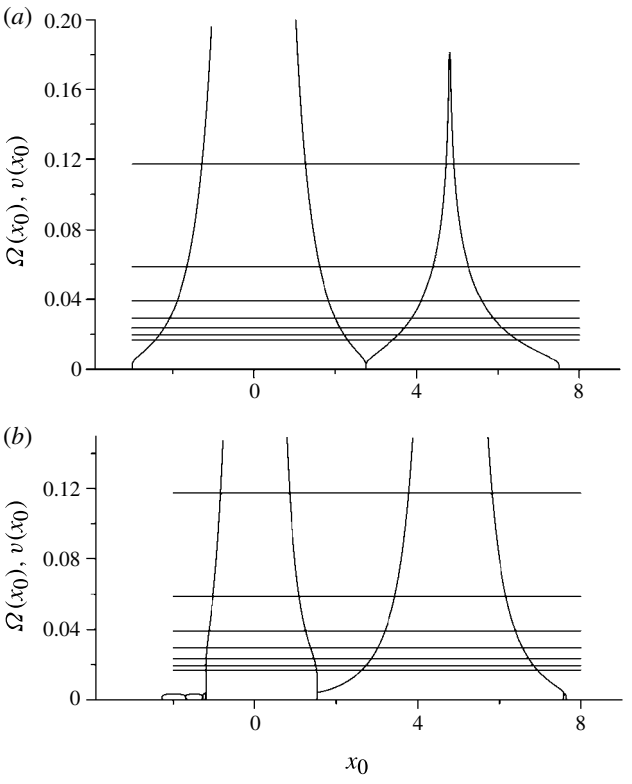

FIGURE 18. Dependences of turnover frequencies Ω (solid lines) and azimuthal velocities v (short-dash lines) of fluid particles versus their initial position on the x-axis in a steady case (triton) with $B = 0.003131$ and $R = 2.4$, for the top (a) and bottom (b) layers. The horizontal lines show the values of frequency $\tilde{\omega}/n$ (n varies from 1 to 7) for the case of figure 5.

used here, alternating depending on the time spent by the particle in the respective domains. The red colour corresponds to the most closed trap, where this particle was located initially and remained during almost 40 000 perturbation periods. The positions of the particle after leaving this domain are shown in blue; it spends about 20 000 perturbation periods in this state, though most of this time is spent in the vicinity of the red trap. Thus, the domain of maximal density of the blue marker can be referred to as a semi-open trap, which the particle leaves from time to time to visit the left loop in the vicinity of the external separatrix. However, at some moment, the particle is captured by the left external trap, where it spends the following 20 000 perturbation periods. The positions of this marker are shown in green.

Returning to the main figure 16(a), we add that the green colour in it corresponds to the marker that started from beyond the atmosphere (external problem). It is captured by the vortex domain, passes through a considerable part of the stochastic sea, which is much larger than that in the bottom layer, and then re-enters the external flow.

Now we consider another interesting example of formation of chaotic regions. The above-described variant of reconnection in the vicinity of a turnover frequency maximum between two separatrices has been much studied, e.g. in Koshel *et al.* (2008); however, it is difficult to realize in the system under consideration, though it is not only reconnections of separatrices of nonlinear resonances induced by perturbation

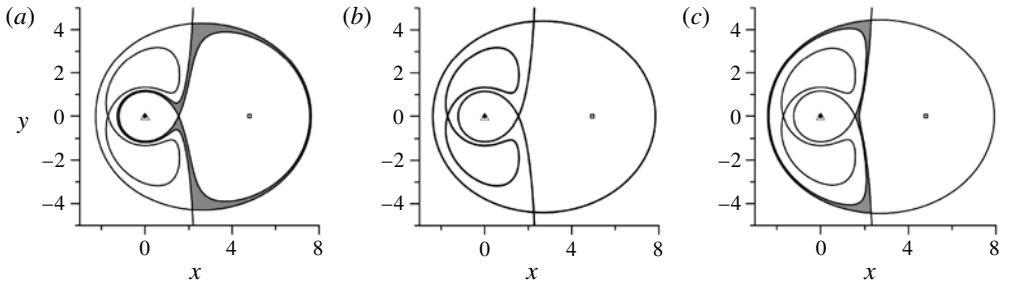

FIGURE 19. Separatrices at: (*a*) $B = 0.003131$, $R = 2.4$; (*b*) $B = 0.002607$, $R = 2.469630$ (reconnection); and (*c*) $B = 0.002408$, $R = 2.5$. Grey shading shows the domain separating the internal and external separatrices.

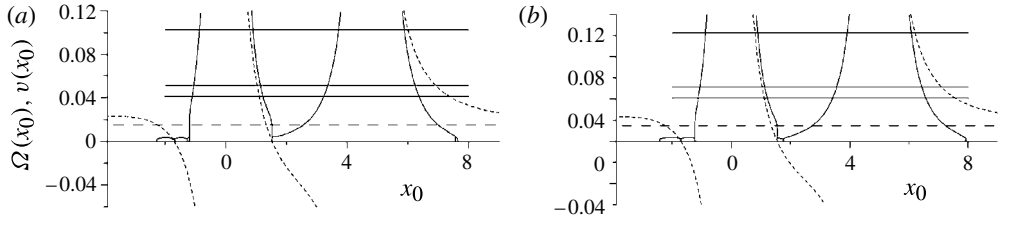

FIGURE 20. Dependences of the turnover frequencies Ω (solid lines) and azimuthal velocities v (short-dash lines) on the initial position of a fluid particle of the bottom layer on the x-axis: (*a*) $B = 0.003131$, $R = 2.4$; (*b*) $B = 0.002408$, $R = 2.5$. These correspond to separatrices in figure 19(*a*,*c*), respectively. The horizontal lines show the values of frequency $\tilde{\omega}/2$, $\tilde{\omega}/4$ and $\tilde{\omega}/5$.

that are possible, but also reconnections of unperturbed separatrices during changes in the sizes of configurations (Sokolovskiy *et al.* 2010). Examples of such reconnection for the bottom layer are given in figures 12(*e*) and 19(*b*) (only separatrices are given in the latter case). The comparison of panels (*a*)–(*c*) in figure 19 clearly shows the process of disappearance of a domain separating the internal and external separatrices during reconnection.

The dependence of turnover frequencies in the vicinity of a reconnection is given in figure 20, where full horizontal lines are drawn at levels of $\tilde{\omega}/2$, $\tilde{\omega}/4$, and $\tilde{\omega}/5$. It is worth mentioning that the perturbation frequency is relatively large in this case and the domains of the main nonlinear resonances (1:1, 1:2, 1:3) form too close to the singular point, a fact which facilitates their rapid narrowing (Ryzhov & Koshel 2010, 2011). Thus, the boundary of the chaotic domain is determined by the position of 1:4 resonance. The second feature of the frequency dependence consists of the presence of a plateau near the separatrix in the domain of the right bottom vortex. In this case, we can expect the formation of a regular barrier preventing fluid particles from penetrating from the near-separatrix stochastic layer into the internal chaotic region. With an appropriately chosen perturbation amplitude, we indeed observe such a barrier and its destruction taking place because separatrices reconnect. Such a scenario of chaotic mixing is illustrated in figure 21.

The results of calculations are given for situations before reconnection and at the moment of reconnection for the internal (markers are initially located in the vortex

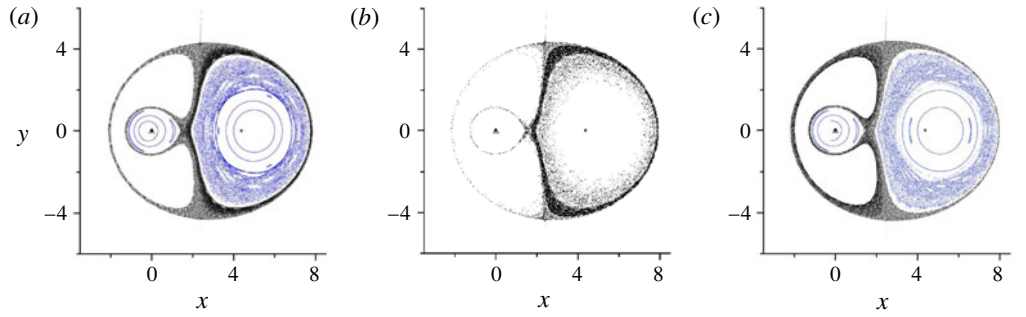

FIGURE 21. Poincaré sections at $\Delta R = 0.185$ for the bottom layer, corresponding to the undisturbed triton behaviour in the vicinity of a reconnection of separatrices (figure 19). The sections are given for values (*a*) $B = 0.003048$, $R = 2.41$, (*b*) $B = 0.002817$, $R = 2.44$, (*c*) $B = 0.002645$, $R = 2.46$. The blue markers are for the internal problem, and the black ones are for the external problem.

domain of the internal separatrix surrounding singular domains) and external (markers are initially located outside the vortex domain in the vicinity of the separatrix) problems. These figures clearly show the barrier of regular behaviour which makes it very difficult for external markers to penetrate into the right vortex domain where mixing of internal markers takes place because of the overlapping of low-order nonlinear resonances. The existence of this barrier is due to the small size of the domain of quasi-linear behaviour of the dependence of turnover frequency.

Now, we will mainly focus on the external problem. Recall that the width of the separatrix stochastic layer reaches a maximum in the vicinity of the hyperbolic point (Gledzer 1999; Zaslavsky 2007).

Thus, at $R = 2.41$ (figure 21*a*), the internal separatrix and the internal part of the external separatrix (along which the external markers penetrate into the vortex domain) are separated by a thin layer with closed trajectories. Exchange of markers takes place within this layer, i.e. the stochastic layers of these separatrices merge together. However, the hyperbolic points are distant in space, and the width of the stochastic layer on the side of the right vortex domain of the internal separatrix is the same as in the absence of the external separatrix.

At the moment of reconnection, which is somewhat shifted because of perturbation and falls to $R \approx 2.44$, the separatrices merge together and hyperbolic points are now located on the same trajectory, resulting in an increase in the thickness of the stochastic layer.

In the Poincaré section corresponding to the value $R = 2.44$ (figure 21*b*), we see that the external markers penetrate into the right vortex domain, but also easily leave it, spending more time in the vicinity of the barrier.

With a further increase in R, a domain separating the separatrices appears again; each stochastic layer becomes thinner (at the same time, they merge within the separation domain), and the barrier again becomes weakly permeable, as can be seen in sections in figure 21(*c*) at $R = 2.46$; the figure also shows internal markers.

Note that the examples of formation of chaotic regions in the vortex atmosphere of the perturbed triton considered here are quite characteristic. The barrier considered here should increase because of extension of the turnover frequency dependence and an increase in the plateau of this dependence, and reconnections of separatrices are observed at several values of parameters. For example, when $R \approx 2.188$, the separatrix

of induced vortices located above or below the x-axis penetrates into the external separatrix.

4. Summary and concluding remarks

Steady solutions in the form of an eccentric roundabout and a triton were found to be very informative objects for use as a background for studying fluid-particle advection. Because of the large number of parameters (geometric characteristics and stratification), even regular advection of fluid particles in the vicinity of these steady vortex structures is very diverse and allows the existence of induced motions of finite and infinite structures, including transport corridors and transport barriers.

The paper also presents analysis of perturbed motions and demonstrates the possibility of formation of chaotic regimes (chaotic advection) at sufficiently large perturbations of stationary configurations. Examples are given of different scenarios of origination and development of chaos. In addition to studying the role of the stochastic layer in the processes of mixing, capture and release of fluid particles by a chaotic domain, conventional for this class of investigations, the role of stratification on these processes was also examined. It was shown that both regular (figures 8–13), and chaotic (figures 15–17, 19 and 21) advection in the top and bottom layer proceed differently. This is of particular importance in applied problems of oceanography, such as mixing of different water masses (in intermediate oceanic layers) or formation of patchy structure in the distribution of plankton or oil pollution (in surface layers). While surface phenomena in the ocean can be monitored with the help of various modern measurement methods (neutral-buoyancy floats, radiometers in satellites), the construction of sound theoretical models for deep-water phenomena are perhaps the only means of study.

This model can also be of use in studying the specific features of jet current meandering (Samelson & Wiggins 2006), detection of barriers to cross-jet Lagrangian transport in the ocean (Budyansky *et al.* 2009), effects of deep convection in the ocean (Marshall & Schott 1999), chaotic stirring and mixing (Abraham & Bowen 2002; Koshel & Prants 2006) and blocking in the atmosphere/ocean (Trenberth & Mo 1985; Duan & Wiggins 1996).

Acknowledgements

This study was supported by RFBR (projects 13-05-00463, 13-05-00131, 11-05-00025), RFBR/CNRS (project 11-05-91052), RF Ministry of Education (Analytical Departmental Goal-Oriented Program 'Development of the Scientific Potential of Higher School', project 2.1.1/554). The authors are grateful to the four anonymous referees for their helpful comments on the manuscript.

REFERENCES

ABRAHAM, E. R. & BOWEN, M. M. 2002 Chaotic stirring by a mesoscale surface-ocean flow. *Chaos* **12**, 373–381.

AREF, H. 1983 Integrable, chaos and turbulent vortex motion in two-dimensional flows. *Annu. Rev. Fluid Mech.* **15**, 345–389.

AREF, H. 1984 Stirring by chaotic advection. *J. Fluid Mech.* **143**, 1–21.

AREF, H. 1986 The numerical experiment in fluid mechanics. *J. Fluid Mech.* **173**, 15–41.

AREF, H., JONES, S. W., MOFINA, S. & ZAWADSKI, I. 1989 Vortices, kinematics and chaos. *Physica* D **37**, 423–440.

AREF, H. & POMPHREY, N. 1980 Integrable and chaotic motions of four vortices. *Phys. Lett.* A **78**, 297–300.

AREF, H. & POMPHREY, N. 1982 Integrable and chaotic motions of four vortices. I. The case of identical vortices. *Proc. R. Soc. Lond.* A **380**, 359–387.

BOATTO, S. & PIERREHUMBERT, R. T. 1999 Dynamics of a passive tracer in a velocity field of four identical point vortices. *J. Fluid Mech.* **394**, 137–174.

BUDYANSKY, M. V., ULEYSKY, M. YU. & PRANTS, S. V. 2009 Detection of barriers to cross-jet Lagrangian transport and its destruction in a meandering flow. *Phys. Rev.* E **79**, 056215.

CHIRIKOV, B. V. 1979 A universal instability of many-dimensional oscillator systems. *Phys. Rep.* **52**, 263–379.

COX, S. M., DRAZIN, P. G., RYRIE, S. C. & SLATER, K. 1990 Chaotic advection of irrotational flows and of waves in fluids. *J. Fluid Mech.* **214**, 517–534.

DUAN, J. & WIGGINS, S. 1996 Fluid exchange across a meandering jet with quasiperiodic variability. *J. Phys. Oceanogr.* **26**, 1176–1188.

ECKHARDT, B. & AREF, H. 1988 Integrable and chaotic motions of four vortices. II. Collision dynamics of vortex pairs. *Phil. Trans. R. Soc. Lond.* A **326**, 655–696.

GLEDZER, A. E. 1999 Mass entrainment and release in ocean eddy structures. *Izv. Atmos. Ocean. Phys.* **35**, 759–766.

GLUHOVSKY, A. & KLYATSKIN, V. I. 1977 On dynamics of flipover phenomena in simple hydrodynamic models. *Dokl. Earth Sci. Sec.* **237**, 18–20.

GRYANIK, V. M. 1988 Localized vortical disturbances – vortex charges and 'vortex threads' in a baroclinic differentially rotating fluid. *Izv. Atmos. Ocean. Phys.* **24**, 1251–1261.

GRYANIK, V. M., SOKOLOVSKIY, M. A. & VERRON, J. 2006 Dynamics of heton-like vortices. *Regul. Chaot. Dyn.* **11**, 383–434.

IZRAILSKY, YU. G., KOSHEL, K. V. & STEPANOV, D. V. 2006 Determining the optimal frequency of perturbation the problem of chaotic transport of particles. *Dokl. Phys.* **51**, 219–222.

IZRAILSKY, YU. G., KOSHEL, K. V. & STEPANOV, D. V. 2008 Determination of optimal excitation frequency range in background flows. *Chaos* **18**, 013107.

JAMALOODEEN, M. I. & NEWTON, P. K. 2007 Two-layer quasigeostrophic potential vorticity model. *J. Math. Phys.* **48**, 065601.

KIMURA, Y. 1988 Chaos and collapse of a system of point vortices. *Fluid Dyn. Res.* **3**, 98–104.

KIZNER, Z. 2006 Stability and transitions of hetonic quartets and baroclinic modons. *Phys. Fluids* **18**, 056601.

KOSHEL, K. V. & PRANTS, S. V. 2006 Chaotic advection in the ocean. *Physics-Uspekhi (Advances in Physical Sciences)* **49**, 1151–1178.

KOSHEL, K. V., SOKOLOVSKIY, M. A. & DAVIES, P. A. 2008 Chaotic advection and nonlinear resonances in an oceanic flow above submerged obstacle. *Fluid Dyn. Res.* **40**, 695–736.

KOZLOV, V. F. & KOSHEL, K. V. 2001 Some features of chaos development in an oscillatory barotropic flow over an axisymmetric submerged obstacle. *Izv. Atmos. Ocean. Phys.* **37**, 378–389.

KUZNETSOV, L. & ZASLAVSKY, G. M. 1998 Regular and chaotic advection in the flow field of a three-vortex system. *Phys. Rev.* E **58**, 7330–7349.

KUZNETSOV, L. & ZASLAVSKY, G. M. 2000 Passive particle transport in three-vortex flow. *Phys. Rev.* E **61**, 3777–3792.

LAMB, H. 1932 *Hydrodynamics*, 6th edn. Dover.

LEONCINI, X., KUZNETSOV, L. & ZASLAVSKY, G. M. 2000 Motion of three vortices near collapse. *Phys. Fluids* **12**, 1911–1927.

LEONCINI, X., KUZNETSOV, L. & ZASLAVSKY, G. M. 2001 Chaotic advection near a three-vortex collapse. *Phys. Rev.* E **63**, 036224.

LEONCINI, X. & ZASLAVSKY, G. M. 2002 Jets, stickiness, and anomalous transport. *Phys. Rev.* E **65**, 046216.

MARSHALL, J. & SCHOTT, F. 1999 Open-ocean convection: observation, theory, and models. *Rev. Geophys.* **37**, 1–64.

MELESHKO, V. V. & VAN HEIJST, G. J. F. 1994 Interacting two-dimensional vortex structures: Point vortices, contour kinematics and stirring properties. *Chaos, Solitons Fractals* **4**, 977–1010.

MELESHKO, V. V. & KONSTANTINOV, M. YU. 1993 *Dynamics of Vortex Structures*, p. 280. Naukova Dumka.

MELESHKO, V. V., KONSTANTINOV, M. YU., GURZHI, A. A. & KONOVALJUK, T. P. 1992 Advection of a vortex pair atmosphere in a velocity field of point vortices. *Phys. Fluids* A **4**, 2779–2797.

NEU, J. C. 1984 The dynamics of a columnar vortex in an imposed strain. *Phys. Fluids* **27**, 2397–2402.

NEUFELD, Z., HAYNES, P. N., GARCÇON, V. & SUDRE, J. 2002 Ocean fertilization experiments may initiate a large-scale phytoplankton bloom. *Geophys. Res. Lett.* **29**, 10.1029/2001GL013677.

NGAN, K. & SHEPHERD, T. G. 1997 Chaotic mixing and transport in Rossby-wave critical layer. *J. Fluid. Mech.* **334**, 315–351.

OLIVA, W. M. 1991 On the chaotic behaviour and non-integrability of four vortices problem. *Ann. Inst. Henri Poincaré* **55**, 707–718.

PÉNTEK, A., TÉL, T. & TOROCZKAI, T. 1995 Chaotic advection in the velocity field of leapfrogging vortex pairs. *J. Phys.* A: *Math. Gen.* **28**, 2191–2216.

PERROT, X. & CARTON, X. 2009 Point-vortex interaction in an oscillatory deformation field: Hamiltonian dynamics, harmonic resonance and transition to chaos. *Discrete Contin. Dyn. Syst.* B **11**, 971–995.

POLVANI, L. M. & PLUMB, R. A. 1992 Rossby wave breaking, microbreaking, filamentation, and secondary vortex formation: the dynamics of a perturbed vortex. *J. Atmos. Sci.* **49**, 462–476.

POLVANI, L. M. & WISDOM, J. 1990 Chaotic Lagrangian trajectories around an elliptical vortex parch embedded in a constant and uniform background shear flow. *Phys. Fluids* A **2**, 123–126.

ROGACHEV, K. A. 2000 Rapid thermochaline transition in the Pacific western subarctic and Oyashio fresh core eddies. *J. Geophys. Res.* **105**, 8513–8526.

ROGACHEV, K. A. & CARMACK, E. C. 2002 Evidence for the trapping and amplification of near-inertial motions in a large anticyclonic ring in the Oyashio. *J. Oceanogr.* **58**, 763–682.

RYZHOV, E. A. & KOSHEL, K. V. 2010 Chaotic transport and mixing of a passive admixture by vortex flows behind obstacles. *Izv., Atmos. Ocean. Phys.* **46**, 184–191.

RYZHOV, E. A. & KOSHEL, K. V. 2011 The effects of chaotic advection in a three-layer ocean model. *Izv., Atmos. Ocean. Phys.* **47**, 241–251.

SAMELSON, R. M. & WIGGINS, S. 2006 *Lagrangian Transport in Geophysical Jets and Waves: the Dynamical Systems Approch*, *Interdisciplinary Applied Mathematics*, vol. 31. p. 147 Springer.

SOKOLOVSKIY, M. A., KOSHEL, K. V. & CARTON, X. 2010 Baroclinic multipole evolution in shear and strain. *Geophys. Astrophys. Fluid Dyn.* **105**, 506–535.

SOKOLOVSKIY, M. A., KOSHEL, K. V. & VERRON, J. 2013 Three-vortex quasi-geostrophic dynamics in a two layer fluid. Part 1. Analysis of relative and absolute motions. *J. Fluid Mech.* **717**, 232–254.

SOKOLOVSKIY, M. A. & VERRON, J. 2000 Four-vortex motion in the two layer approximation: integrable case. *Regul. Chaot. Dyn.* **5**, 413–436.

SOKOLOVSKIY, M. A. & VERRON, J. 2002*a* New stationary solutions of the three-vortex problem in a two-layer fluid. *Dokl. Phys.* **47**, 233–237.

SOKOLOVSKIY, M. A. & VERRON, J. 2002*b* Dynamics of the triangular two-layer vortex structures with zero total intensity. *Regul. Chaot. Dyn.* **7**, 435–472.

SOKOLOVSKIY, M. A. & VERRON, J. 2004 Dynamics of the three vortices in two-layer rotating fluid. *Regul. Chaot. Dyn.* **9**, 417–438.

SOKOLOVSKIY, M. A. & VERRON, J. 2006 Some properties of motion of $A + 1$ vortices in a two-layer rotating fluid. *Russ. J. Nonlinear Dyn.* **2**, 27–54.

THOMSON, W. 1867 On vortex atoms. *Phil. Mag.* 4 **34**, 15–24.

TRENBERTH, K. F. & MO, K. C. 1985 Blocking in the Southern Hemisphere. *Mon. Wea. Rev.* **113**, 3–21.

VELASCO FUENTES, O. U. 1994 Propagation and transport properties dipolar vortices on a γ-plane. *Phys. Fluids* **6**, 3341–3352.

VELASCO FUENTES, O. U., VAN HEIJST, G. J. F. & CREMERS, B. 1995 Chaotic advection by dipolar vortices on a γ-plane. *J. Fluid Mech.* **291**, 139–161.

YANG, H. 1993 Chaotic mixing and transport in wave systems and atmosphere. *Intl J. Bifurcation Chaos* **3**, 1423–1445.

YANG, H. 1996*a* The subtropical/subpolar gyre exchange in the presence of annually migrating wind and meandering jet: water mass exchange. *J. Phys. Oceanogr.* **26**, 115–139.

YANG, H. 1996*b* Lagrangian modelling of potential vorticity homogenization and the associated front in the Gulf Stream. *J. Phys. Oceanogr.* **26**, 2480–2496.

YANG, H. 1998 The central barrier, asymmetry and random phase in chaotic transport and mixing by Rossby waves in a jet. *Int. J. Bifurcation Chaos* **8**, 1131–1152.

YANG, H. & LIU, Z. 1994 Chaotic transport in a double gyre ocean. *Geophys. Res. Lett.* **21**, 545–548.

YANG, H. & LIU, Z. 1997 The three-dimensional chaotic transport and the great ocean barrier. *J. Phys. Oceanogr.* **27**, 1258–1273.

ZASLAVSKY, G. M. 2007 *The Physics of Chaos in Hamiltonian Systems*, 2nd edn, p. 316. Imperial College Press.